Ab initio study of decohesion properties in oxide/metal systems

J. I. Beltrán*

Université de Mons-Hainaut, Mons 7000, Belgium and Instituto de Ciencia de Materiales de Madrid, CSIC, Madrid 28049, Spain

M. C. Muñoz

Instituto de Ciencia de Materiales de Madrid, CSIC, Madrid 28049, Spain

(Received 12 June 2008; revised manuscript received 13 October 2008; published 18 December 2008)

Several studies of the decohesion properties of various oxide/metal systems have been performed recently by *ab initio* calculations. However, the use of different computational methods, which involve diverse approximations, energy functionals, or calculation conditions, makes the identification of general trends difficult. In the present work, a broad range of interfaces between an ionic oxide (Al_2O_3, ZrO_2, HfO_2, and MgO) and a metal [either transition metal (TM) or Na], has been investigated systematically in order to find correlations among the work of separation (Wsep) and the intrinsic properties of the interface, such as the crystal structure, the strain conditions, or the electronic properties of both constituents. Our main result is that the calculated Wsep adjusts very accurately to a parabolic dependence on the summed surface energies of the metal and the oxide, regardless of the oxide and metal components, crystal lattices, interface orientations, and atomic terminations. Furthermore, Wsep is mostly determined by the surface energies although for interfaces involving nonpolar oxide surfaces the contribution of the interfacial energy is not negligible. The strongest adhesion is found for interfaces formed by polar surfaces and bcc TM, e.g., the Wsep of $ZrO_2(001)_O/TM$ interfaces changes almost by a factor of 2 depending on whether the TM has bcc or fcc structure. In addition, a correlation between the strain conditions of the equilibrium interface structure and the adhesion properties has been obtained. Finally, in order to predict metal/oxide systems whose mechanical properties are reinforced by the plastic deformation of the metal, we examine the expected behavior of the system beyond the elastic regime in the light of the calculated adherence at the interface. The comparison with the scarcely available experimental data provides good agreement for both the Wsep and the qualitative prediction of mechanical reinforcement.

DOI: 10.1103/PhysRevB.78.245417 PACS number(s): 68.37.Nq, 68.55.−a, 71.20.Tx, 71.70.Ej

I. INTRODUCTION

Composite materials, constituted by oxides and metals, are of great importance for a wide range of technological applications such as: heterogeneous catalysis, multifunctional devices, fuel cells, or thermal barrier coatings.[1,2] Their technological interest arises from the possibility to obtain materials with tailored properties which may differ from those of their constituents. In addition, the combination of dissimilar materials may allow to better exploit the characteristics of both constituents.[3] The composite mechanical properties are determined by a complex balance among interactions both at the mesoscopic and atomistic level and in general they are intimately related to the formation of a good and strong metal/ceramic interface. For example, in cermet composites, metallic particles are embedded in a ceramic matrix in order to reinforce the composite mechanical properties by plastic deformation of the metal.[4] Such deformation provides a mechanism at the mesoscopic level, crack blunting, to reduce the energy of a propagating crack in the cermet. Even if there is a large lattice mismatch between the metal and the ceramic at the atomistic scale, reinforcement by crack blunting takes place in a few systems such as Al_2O_3/M (M=Ni, Cu, and Au) or ZrO_2/Nb.[5,6] However, for most ceramic/metal composites the reinforcement of the ceramic brittleness does not occur due to the failure of the system at the interface between the ceramic and the metal.[7] Therefore, the mechanical properties of cermet materials are largely dependent on the metal/ceramic interface adhesion.

Atomistic theoretical studies of various oxide/metal systems, based on *ab initio* calculations, have been performed in order to describe at the atomic level the interactions at the interface[8,9] and to understand the origin of the experimental fracture energy data.[10,11] Nevertheless, most calculations refer to a specific system and for particular thickness and growth conditions. They are mainly focused on either isolated atoms[12] or single monolayers[13] of the Al_2O_3/Ni and ZrO_2/M (M=Cu, Pd, and Pt) systems,[14] making it difficult to achieve general trends for ceramic/metal interfaces. To our knowledge, the only systematic investigations were the studies of Bogicevic *et al.*[15] on the adsorption of metal overlayers on aluminum oxide, of Siegel *et al.*[16] on different ceramic/Al systems including Al_2O_3, carbides, and nitrides, and our previous studies on metal-ZrO_2 interfaces.[6,7,17–19] In the present work, we attempt to correlate the work of separation (Wsep)—the parameter characterizing the mechanical response of the composite—with the inherent properties of the metals and oxides forming the interface, extending the up to date results mainly focused on α-Al_2O_3. Despite several approximations needed in order to investigate a wide range of systems, we are able to obtain general trends at the mesoscopic level which agree qualitatively with fracture energy measurements.

TABLE I. Lattice parameter (in Å), bulk modulus (in GPa), and cohesive energy (in eV) for the constituent metals of the ceramic/metal interfaces. Present results are compared with experiments and the experimental cohesive energy is obtained from Ref. 33. At the bottom of the table we can see the dispersion of our results with respect to the experimental measures.

		a/c			B_0			E_{coh}	
System	Sym	Present work	Expt.	Ref.	Present work	Expt.	Ref.	Present work	Expt.
Al	fcc	4.044	4.032	25	79	79	25	3.96	3.39
Rh	fcc	3.868	3.798	25	247	269	25	6.63	5.75
Cu	fcc	3.665	3.603	25	143	142	25	4.35	3.49
Ag	fcc	4.172	4.069	25	89	109	25	3.25	2.95
Ni	fcc	3.550	3.519	26	183	180	26	5.50	4.44
Pd	fcc	4.007	3.881	25	148	195	25	4.32	3.89
Pt	fcc	4.025	3.921	27	221	230	27	6.11	5.84
Mo	bcc	3.188	3.145	28	239	230	27	6.19	6.82
Na	bcc	4.201	4.225	25	6.2	7.5	25	1.01	1.11
Nb	bcc	3.315	3.250	27	136	170	27	6.28	7.57
Ta	bcc	3.324	3.300	29	197	200	27	8.48	8.10
W	bcc	3.197	3.160	29	285	310	27	8.28	8.90
Mg	hcp	3.230	3.210	30	34	35	30	1.56	1.51
		5.240	5.210						
Y	hcp	3.700	3.650	29	47	41	27	4.32	4.37
		5.850	5.730						
Zr	hcp	3.250	3.230	31	86	97	31	6.54	6.25
		5.210	5.150						
Hf	hcp	3.200	3.190	32	100	110	32	7.30	6.44
		5.050	5.040						
$\frac{\sqrt{\Sigma(\frac{theor-expt.}{expt.})^2}}{N}$		1.016			0.880			1.130	

II. THEORETICAL METHODOLOGY

The theoretical calculations have been performed with the *ab initio* SIESTA code[20] based on the density-functional theory (DFT),[21,22] using norm-conserving pseudopotentials and the generalized gradient approximation (GGA) in the Perdew-Burke-Ernzerhof scheme for the exchange and correlation term.[23] A linear combination of strictly localized numerical atomic orbitals constitutes the basis set. In our calculations the valence states for all transition metals (TMs) were described by double-zeta s and d shells and single-zeta p shell after polarizing the s shell.[22] The basis for oxygen and sodium comprised double-zeta s and p shells plus a single-zeta (polarized) d shell. Brillouin-zone (BZ) integrations were performed over a Monkhorst-Pack grid of the BZ of the primitive cell.[24] The mesh size depends on the material and is typically $8\times8\times8$ for bulk metals, $6\times6\times6$ for cubic oxides, and $6\times6\times2$ for α-Al_2O_3. For bulk calculations structural optimization was allowed until the residual forces in all the atoms were smaller than 0.05 eV/Å. Tables I and II summarize the calculated equilibrium lattice parameter, bulk modulus, and crystal cohesive energy of the bulk metal and oxide phases, together with the experimental values. As expected from the GGA approximation, the calculated lattice parameters are slightly larger than the experimental values, with deviations below 2%, while the bulk moduli and cohesive energies are reasonably well reproduced. Further, in the case of Ni we obtained a magnetic moment of $0.6\mu_B$ in good agreement with previous calculations and experiments. For the oxides, the gap width is underestimated compared to the experimental values, a characteristic of DFT.

The interfaces have been modeled within a slab approach with periodic boundary conditions. The equilibrium structures were obtained relaxing both the cell size and the atomic positions until the forces in all the atoms were less than 0.1 eV/Å and typically smaller than 0.05 eV/Å. The supercell BZ was sampled using a Monkhorst-Pack tensor whose related in-plane K-grid cutoff is always larger than 10.5 Å, with no translation along the perpendicular interface vector. The cut-off value corresponds at least to the $3\times4\times1$ Monkhorst-Pack tensor[24] for the largest interface real-space cell and typically takes the value of $10\times10\times1$. Details on the computational conditions and parameters can be found elsewhere.[17–19]

The initial configuration is formed by straining the metal to match the two-dimensional (2D) ceramic unit cell parallel to the interface. Therefore, only the metal is either compressed or stretched. The area strain parameter ΔA_i is defined as the ratio of the (2D) unit-cell areas at the interface and at the ideal bulk termination for both ceramic (i=CER) and metal (i=MET). Thus, in the initial configuration $\Delta A_{CER}=0$. Relaxations, both in plane and perpendicular to the interface,

TABLE II. Same as Table I for the oxides forming the interfaces. Present results are compared to earlier calculations and experiments. Calculated cohesive energy is compared to the experimental formation enthalpy of the oxide from Refs. 33 and 54.

Oxides		a	c	B_0	E_{coh} (eV)	Ref.
α-Al_2O_3	Present/GGA	4.85	13.16	213	15.27	
	PW/PW91	4.79	13.08	246		34
	PW/LDA	4.72	12.86	239		34
	OLCAO	4.83	12.61	242		35
	Expt.	4.76	13.00	253	17.37	36–38
MgO	Present/GGA	4.27		118	5.51	
	GGA	4.24		161		25
	GGA/PBE	4.28		140		39
	LDA	4.16		182		25
	GGA/ECP	4.27		151		40
	GGA/PAW	4.25		151		40
	Expt.	4.21		152	6.23	25 and 39
c-HfO_2	Present/GGA	5.11		254	10.85	
	GGA	5.15		257		41
	GGA/PW91	5.00				42
	LDA	5.14		280		43
	LDA	5.09		289		41
	Expt.	5.08		280	11.52	42 and 44
c-ZrO_2	Present/GGA	5.16		235	10.42	
	GGA/PW91	5.16				45
	LDA	5.08				45
	GGA	5.09				46
	LDA	5.04				47
	SC-TB	5.02				48
	HF	5.15				49
	Expt.	5.09		194–220	10.74	44 and 50–53

are allowed for the two components: the metal and the ceramic. In general, at the equilibrium configuration the ceramic material experiences some stress although almost all the lattice mismatch is adjusted at the metal side of the junction (see below). We allow relaxation of both constituents since composite materials usually show a granular structure where the lattice mismatch can be adsorbed by both the metal and the ceramic. In fact, cermets with large lattice mismatch between their constituents, as Al_2O_3 and ZrO_2/Nb, show atomic faceting with regions of abrupt interfaces at the atomic scale instead of planar sharp interfaces with a 2D unit cell corresponding to that of either the metal or the oxide.[6] Besides, surfaces of thin layers and nanoparticles of oxides may present structural parameters slightly different to those of the corresponding bulk crystals.[7,55]

We have performed two different kinds of calculations: the first corresponds to a supercell geometry including two slabs formed, respectively, by the metal and the ceramic, and the second model corresponds to the free overlayers of metals on top of the ceramic surface. In the former there are two identical interfaces in the supercell so it mainly describes interfaces between bulk systems as those present in cermets, solid metal interfaces, composites, etc. In this case, the selected materials have always a 2D unit-cell area misfit smaller than 10%, except for two interfaces formed by Al_2O_3 which compensate metal stretching with ceramic squeezing. A larger mismatch may lead to unphysical results since 10% area mismatch corresponds to 3%–4% differences of lattice parameters. It is expected that in this range of mismatch between ceramic and metal lattice parameters, the actual structures of the interfaces will present large coherent regions separated by misfit dislocations or small incommensurate disordered regions. In the second type of calculations, only performed for ZrO_2 and bcc metals, there is just one ceramic/metal interface and a free metal surface created by including a vacuum region large enough to inhibit interactions between the two terminating surfaces of the slab. Thus, this supercell geometry may model epitaxial metal film growths on ceramics as well as cermets with large lattice mismatch, which, as discussed above, may present faceted interfaces. Area mismatches up to 26%, which correspond to around 12% variation in the metal and oxide lattice parameters, have been considered. These calculations are performed in order to investigate the influence of the interface adhesion properties on the enhancement of the fracture energy by the bridging mechanisms reported experimentally.[6] In that work, a clear correlation between the atomically matched interface facets and the observed mechanical enhancement mechanism in the composite materials has been established.

In order to quantify the adhesion properties with *ab initio* atomic simulations we have calculated the Wsep. Wsep is defined as the energy required to break interface bonds and thus is the reversible work needed to separate the interface into two free surfaces if the plastic and diffusional degrees of freedom are suppressed.[17] Two equivalent relations define the Wsep:

$$\mathrm{Wsep} = (E_{\mathrm{MET}} + E_{M_xO_y} - E_{\mathrm{INT}})/(2A) = \sigma_{\mathrm{MET}} + \sigma_{M_xO_y} - \gamma, \quad (1)$$

where E_{MET} and $E_{M_xO_y}$ are, respectively, the total energy of the isolated relaxed metal and oxide M_xO_y systems, E_{INT} is the total energy of the complete metal/oxide structure, and A is the cross-sectional area. σ_{MET} and $\sigma_{M_xO_y}$ denote metal and oxide surface energies, respectively, and γ is the interfacial energy. The calculated Wsep can be compared with the experimental decohesion contribution (Γ) to the fracture energy, which characterizes the fracture properties of a brittle joint interface.[4]

Equation (1) shows that Wsep is also related to the interface γ and surface σ free energies, and therefore it can be analyzed in terms of the stability of the surfaces of both the metal and the oxide. To calculate the surfaces stabilities the procedure described in Refs. 17 and 56–59, which combines first-principles calculations with a thermodynamic approach, has been followed. There are two types of oxide slabs: stoichiometric (ST), with a number of atoms equal to an integer number of oxide formula units, and nonstoichiometric (NST) slabs. Surface and interface energies corresponding to NST interfaces can only be calculated as a function of the chemical potential of either the cation (μ_M) or the O (μ_O). Using the microcanonical ensemble, γ and σ are given as a function of μ_O by

$$\mu_{M_xO_y} N_{M_xO_y} = \frac{(N_M G^{\mathrm{bulk}}_{M_xO_y})}{x} + \mu_O\left(N_O - \frac{N_M y}{x}\right),$$

$$\gamma = \frac{E_{\mathrm{INT}} - \mu_{M_xO_y} N_{M_xO_y} - \mu_{\mathrm{MET}} N_{\mathrm{MET}}}{2A},$$

$$\sigma = \frac{(E_{M_xO_y} + E_{\mathrm{MET}}) - \mu_{M_xO_y} N_{M_xO_y} - \mu_{\mathrm{MET}} N_{\mathrm{MET}}}{2A}. \quad (2)$$

where x and y are the number of cation and O atoms per oxide formula unit, respectively, $G^{\mathrm{bulk}}_{M_xO_y}$ is the Gibbs free energy, and N_i is the number of atoms of type i ($i = M, O, \mathrm{MET}$). The allowed range of μ_O is constrained by the chemical potential of the O_2 molecule $\mu^{\mathrm{gas}}_{O_2}$ and the formation Gibbs free energy of the M_xO_y oxide, $\Delta G^f_{M_xO_y}$. Therefore, μ_O fulfills the relation,[17,58]

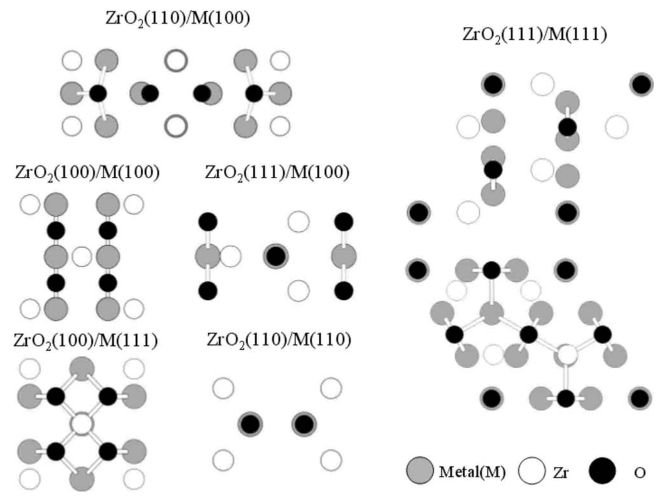

FIG. 1. Top view of the c-HfO_2/metal or c-ZrO_2/metal interfaces modeled for different metals and relative crystallographic orientations showing the metal-oxygen interface bonds. Only the Zr, O, and metal planes closer to the interfaces are represented. The relative crystal orientations of the ceramic and the metal are specified for each case.

$$\frac{1}{y}\Delta G^f_{M_xO_y} < \mu_O - \frac{1}{2}\mu^{\mathrm{gas}}_{O_2} < 0.$$

Hereafter, the chemical potential will be given relative to the binding energy of molecular oxygen, $\Delta\mu_O = \mu_O - \frac{1}{2}\mu^{\mathrm{gas}}_{O_2}$.

III. INTERFACE GEOMETRY

We have performed a systematic study of the dependence of the adhesion properties on the choice of the metal at extended 2D interfaces. The selection of metals for each particular ceramic interface has been based on the value of the 2D lattice misfit. We have only considered low index surfaces with small commensurable unit cells and tried to analyze the influence of two effects: the lattice orientations, which imply changes in both structure and oxide polarity, and the metal electronic configuration. To this end, we have studied Na and transition metals with low and high occupancy of the *d* band, namely, Nb, Mo, Ta, and W on one side and Ni, Cu, Rh, Pd, Ag, and Pt on the other. It should be noted that a different bulk crystal structure corresponds to each group, bcc for Na and the TM of low *d*-band occupancy and fcc for the rest.

The unit cells used in our c-ZrO_2/metal and c-HfO_2/metal calculations appear in Fig. 1. All models correspond to fcc metals except the c-ZrO_2(111)/metal(100) case (middle center in the Fig. 1), which refers to bcc metals. The unit cells corresponding to the interfaces formed by α-Al_2O_3 and MgO are represented in Fig. 2. For Al_2O_3 the metals investigated are all bcc, while for MgO, Na is bcc and Ag fcc. The figure shows the unrelaxed configuration of our calculations where the strain induced by the misfit is assigned to the metal. For the oxide polar surfaces, where both metal and O terminations are possible, we focus the analysis on the O-ended cases although some metal terminations are

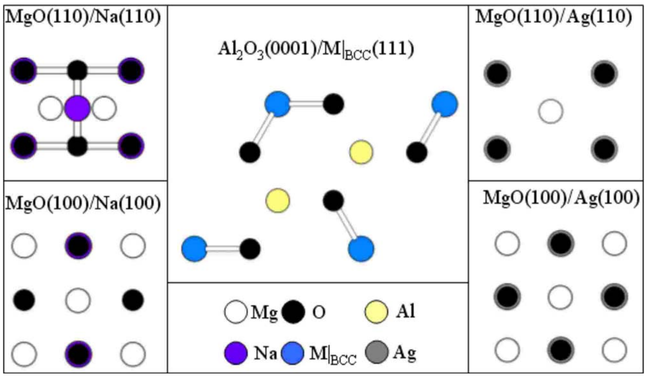

FIG. 2. (Color online) Same as Fig. 1 for the $Al_2O_3(0001)_O$/metal(111) and MgO/metal systems.

also investigated. All the interfaces are modeled by considering that interface reactions do not take place, and the adhesion properties are calculated under the elastic regime; so dissipative processes are not taken into account. Moreover, the calculations model ideal interfaces without defects as, for example, vacancies or interstitials.[60]

IV. WORK OF SEPARATION

A summary of our results for interfaces with less than 10% area misfit between constituents is shown both in Table III for the NST interfaces and in Table IV for the ST slabs. Table V includes similar information for the interfaces with large mismatch (more than 10%). In the tables it is shown that the initial strain assigned to the metal is, after relaxation, distributed between both the metal and the oxide structures. Nevertheless, the final ceramic strain, which depends on the particular ceramic and crystal orientation, is usually smaller than that of the metal, never exceeds 5% (13%) and commonly corresponds to 2%–3% (5%–6%) for interfaces with nominal area mismatch of less (more) than 10%. In the tables, instead of the actual interface ceramic-metal bond, the ratio between the interface bond length and the sum of the respective ionic radii is shown. Note that for some interfaces there is a large dispersion of relative atomic positions within the 2D unit cell, as can be inferred from the large differences between the shortest metal-oxygen bond length (represented by Δd) and the mean bond length ($\langle\Delta d\rangle$). The disparity of the considered structures of ceramic and metals makes it difficult to establish trends among structures. Even for a given ceramic, i.e., ZrO_2, there is a large variety of 2D interface unit cells, which differ in the number of metal-O bonds, in the metal to O coordination, and/or in the amount of strain. In addition, some interfaces involve Zr terminations or nonpolar ZrO_2 surfaces and thus the metal-Zr interaction also contributes to the adhesion.

Even though a set of general common properties can be sketched for the interfaces studied, some of them are not

TABLE III. We show for the interfaces with less than 10% mismatch and constituted by a NST ceramic slab: the out-of plane orientation of both constituents, the ratio between the shortest bond length between the metal and the ceramic (either with an anion or cation), and the sum of the ionic radii of the atoms forming the bond (Δd), and the same ratio taking the mean bond length instead of the shortest one ($\langle\Delta d\rangle$); the difference between the average interface Mulliken charge and the bulk charge (ΔQ) for the ceramic and metal atoms at the interface; the ratio of the 2D unit-cell areas at the interface and at the ideal bulk termination (ΔA) for both ceramic and metal; and the work of separation (Wsep, in J/m^2).

NST ceramic	Δd	$\langle\Delta d\rangle$	ΔQ_{CER}	ΔQ_{MET}	ΔA_{CER}	ΔA_{MET}	Wsep
$Al_2O_3(0001)_O$/							
Ta(111)	0.99	1.03	−0.02	−0.77	1.00	1.07	10.47
W(111)	1.04	1.06	−0.05	−0.57	0.97	1.12	9.76
Mo(111)	1.02	1.04	−0.09	−0.45	0.97	1.12	9.58
Nb(111)	1.02	1.06	−0.08	−0.65	1.02	1.09	9.26
$ZrO_2(100)_O$/							
Ni(100)	0.92	0.92	−0.16	−0.28	1.01	1.06	5.74
Cu(100)	0.97	0.97	−0.17	−0.27	1.02	1.01	5.08
Rh(111)	0.89	0.89	−0.17	−0.22	1.01	1.03	4.02
Pt(111)	0.90	0.92	−0.21	−0.30	1.05	1.00	3.37
$ZrO_2(100)_{Zr}$/							
Ni(100)	1.05	1.05	0.42	0.19	0.99	1.05	5.01
Cu(100)	1.10	1.10	0.57	0.10	1.02	1.01	3.66
HfO_2/Ni(100)							
$HfO_2(100)_O$	0.92	0.93	−0.14	−0.25	1.01	1.04	6.26
$HfO_2(100)_{Hf}$	1.03	1.03	0.34	0.24	0.99	1.02	5.54

TABLE IV. Same as Table III for interfaces constituted by ST ceramics.

ST ceramic	Δd	$\langle \Delta d \rangle$	ΔQ_{CER}	ΔQ_{MET}	ΔA_{CER}	ΔA_{MET}	Wsep
$ZrO_2(111)_O$/							
Ta(100)	0.99	1.01	−0.03	−0.21	0.95	0.99	2.23
Nb(100)	1.06	1.08	−0.08	−0.14	0.96	1.00	1.84
Ni(111)[a]	0.92	0.94	−0.15	−0.12	1.05	0.98	1.12
Ni(111)[b]	0.93	0.97	−0.08	−0.13	1.04	0.94	1.28
$ZrO_2(110)$/							
Ni(110)	0.93	0.93	−0.07	−0.12	0.97	1.03	2.15
Cu(110)	0.98	0.98	−0.07	−0.10	1.01	1.00	1.43
Ni(001)	0.95	0.97	−0.08	−0.18	0.99	0.98	0.94
Cu(001)	1.04	1.05	−0.09	−0.16	1.02	0.95	0.71
HfO_2/Ni							
(110)/(110)	0.93	0.93	−0.04	−0.09	0.98	1.01	2.09
$(111)_O$/(111)	0.94	0.97	−0.05	−0.09	0.96	0.93	1.29
(110)/(001)	0.96	0.98	−0.04	−0.15	1.00	0.98	1.07
MgO/Ag							
(110)/(110)	0.86	0.86	−0.05	−0.12	0.96	1.04	1.10
(100)/(100)	0.99	0.99	−0.04	−0.06	0.94	1.03	0.72
MgO/Na							
(110)/(110)	1.10	1.10	−0.09	0.14	1.01	1.08	0.65
(100)/(100)	1.16	1.16	−0.04	0.20	0.97	1.04	0.17

[a]Aligned with in-plane directions ZrO_2[1−10]/Ni[1−10] (Ref. 61).
[b]Aligned with in-plane directions ZrO_2[1−34]/Ni[0−44] (Ref. 62).

TABLE V. Same as Tables III and IV for the interfaces with more than 10% mismatch between a metal overlayer and ZrO_2.

NST ceramic	Δd	$\langle \Delta d \rangle$	ΔQ_{CER}	ΔQ_{MET}	ΔA_{CER}	ΔA_{MET}	Wsep
$ZrO_2(100)_O$/							
Ta(100)	0.97	1.02	−0.07	−0.63	0.97	1.16	10.88
W(100)	1.03	1.08	−0.06	−0.67	0.91	1.19	9.61
Mo(100)	1.03	1.05	−0.10	−0.50	0.96	1.26	9.08
Nb(100)	0.99	1.05	−0.14	−0.49	0.97	1.17	9.07
Rh(100)	0.85	0.86	−0.25	−0.22	1.05	0.93	4.57
Pd(100)	0.88	0.89	−0.27	−0.17	1.06	0.88	2.91
$ZrO_2(111)_O$/							
W(100)	1.01	1.10	−0.05	−0.24	0.92	1.03	2.28
Mo(100)	1.02	1.08	−0.06	−0.19	0.92	1.04	1.85
Cu(111)	0.97	1.03	−0.17	−0.11	1.07	0.94	0.62
$ZrO_2(110)$/							
Rh(100)	0.92	0.93	−0.15	−0.11	1.05	1.31	1.94
Pt(100)	0.91	0.92	−0.18	−0.08	1.13	1.31	1.59
Pd(100)	0.98	0.99	−0.10	−0.05	1.00	1.16	0.50

explicitly deduced from the tables such as the metallic character of the interfaces or the rapid decay of the interface effects, characteristics also observed for the adsorption of single metal atoms and layers studied by other authors.[63] Another common feature is the ionic nature of the metal-oxygen bonds, which in all cases involve O charge depletions with respect to the bulk oxide.[7] Although certain ionic character may be assigned to the metal-cation bonds, because of their different electronegativity, the bonds are mainly formed by hybridization of the electronic states and thus in general the electronic bond charge is shared by both metals.

The work of separation cannot be universally correlated with the average interface Mulliken charge due to the diversity on the number of bonds per unit area and the various metal-O and metal-metal pair coordination numbers present at the different interfaces. Even more, bonds with ionic or metallic character show different electronic charge distributions and consequently a different variation in the Mulliken charge. Nevertheless, for a fixed oxide interface the correlation is clear and in general large electron transfer from the metal to the oxygen atoms or large charge shared in the metal-cation bonds corresponds to large Wsep. The fluctuations are due to the coexistence of bonds of different strength in the interface. Therefore, the largest values of Wsep correspond to interfaces with the highest number of strong metal-oxide bonds per unit area, i.e., to the largest charge transfer or largest metal-metal electron hybridization.

The relation between Wsep and the bond lengths is more intricate, partly due to the presence of individual short bond lengths (strong bonds) coexisting with weaker bonds at some interfaces. In general, the strongest interactions correspond to the bcc metals forming interfaces with $Al_2O_3(0001)$ and $ZrO_2(001)$, while the weakest ones are found for MgO both with alkaline and noble metals.

Tables III–V show an important dispersion of Wsep being the difference between the two extreme values larger than an order of magnitude. Nevertheless, these values correspond not only to different metals and different ceramic oxides but also to different lattice orientations which imply variations in lattice structure, polar character of the ceramic surface, and therefore different electronic density distribution. Although the matching of the metal and ceramic structures at the interface has a determinant influence on the adhesion, especially regarding the extended 2D interfaces, some trends for Wsep can also be tracked down concerning the electronic properties. First, for a common number of valence electrons, increasing the metal atomic number (Z) enhances Wsep. Second, lower occupancies of the d band (bcc structures) lead to stronger adhesions, while the adhesion for the Na [*sp* valence band (VB)] is very weak. Third, there is a general common property showed by all the interfaces studied; the Wsep for NST oxide surfaces is substantially larger than that corresponding to ST surfaces. In particular, interfaces formed between NST surfaces of oxide ceramics and transition metals of low d-band occupancy and bcc crystal structure, namely, Nb, Mo, Ta, and W, present a very good adhesion with Wsep of the order of 10 J/m^2. On the other side we find that interfaces composed by ST oxide surfaces and metals with high occupancies of the d band and fcc structure as Cu, Ni, Pd, Pt, Ag, and Rh exhibit much lower Wsep. In fact, most ST ceramic surfaces correspond to nonpolar terminations except for the c-$ZrO_2(111)_O$ and c-$HfO_2(111)_O$ polar surfaces ended in a single O-layer, which is a particular case of polar nondivergent surface.[64] For these particular cases, although there is an alternation of positively and negatively charged planes so that the charge at the topmost surface plane is not compensated, the entire ceramic slab has the proper stoichiometry; so these surfaces are stable similarly to the nonpolar ones.

V. COMPARISON WITH PREVIOUS EXPERIMENTAL RESULTS

In the following, we will compare our results with previous theoretical and experimental works considering each ceramic oxide separately.

Much of the early work on metal/zirconia adhesion was based on the study of the wetting phenomena and the energetics of the interfaces described by the contact angle θ. The work of adhesion (Wadh) and the contact angle are related through the surface energy of the liquid metal, σ_L, by the Young-Dupré equation, $\text{Wadh}=\sigma_L[1+cos(\theta)]$ (see Ref. 65). The exact value of Wadh that corresponds to wetting experiments is generally lower than that obtained by *ab initio* studies due to the geometry differences as explained in Ref. 65. Nevertheless, for a given oxide the relative trends of variation can be compared. Wettability experiments with different metal melts,[17] using ZrO_2 single crystals as substrate, find a different wetting behavior when comparing ST and NST ZrO_2 substrates. The measured θ ranges from 65° to 150° for ST ZrO_2, while for NST it is reduced from 60° to 130°. The contact angle reduction in NST ZrO_2 indicates that the adhesion is stronger, as we have also obtained (see Tables III–V).

Although *ab initio* studies of the ceramic/metal interface adhesion are quite recent, which implies that in general there are not many results, by far the most studied systems have been those involving α-Al_2O_3 and Nb, Ni, and Al as metals. For them, an important number of theoretical calculations and experimental works can be found in the literature. Theoretical calculations performed on the $Al_2O_3(0001)_O/Nb(111)$ interface[9] show the formation of a strong interface with a Wsep of 9.8 J/m^2 when cleaving the Al_2O_3 at the O plane and of 2.7 J/m^2 when cleaving at the Al one. This result compares nicely with our value of 9.3 J/m^2 for the O termination, as well as with the close values that we obtain for the bcc metals Mo, W, and Ta with similar electronic structure than Nb.

Finally, concerning MgO, we have performed calculations only for Na and Ag with similar lattice parameter than that of the ceramic. Ag has been largely studied by *ab initio* calculations, with special emphasis on the effect of the different interface positions on the value of Wsep, as shown in Table VI.

We can see that our calculated Wsep is lower than those obtained previously, but it is the closest to the experimental Wsep. Previous theoretical work[71] has found that alkali metals, and particularly 0.5 and 0.25 ML of Na deposited on MgO (001) show a weak physisorption with higher interaction at the O on-top site than at the Mg site. We obtain

TABLE VI. Values of Wsep (J/m^2) for MgO/Ag depending on the relative interface position of the Ag compared to previous calculations (Refs. 66–69) and experimental measurements (Ref. 70).

References	On-top Mg	On-top O
Li	0.54	
Schönberger	0.70	1.60
Heifets	0.63	0.81
Hong	1.08	1.90
Ours	0.27	0.72
Experiment		0.45

similar results with the values of 0.65 and 0.17 J/m^2 for Na on top of O and Mg, respectively, which in addition are among the lowest Wsep values for all the systems studied here. From wetting measurements[72] and references therein, the wetting angles for all nonreactive MgO/metal interfaces are over 90°, therefore indicating the low interaction at the interface.

In summary, the calculated values of Wsep in Tables III–V show a reasonable quantitative agreement with the available experimental and theoretical data.

VI. WORK OF SEPARATION VS METAL PROPERTIES

If we restrict to a particular ceramic oxide structure, c-ZrO_2 and c-HfO_2, additional dependences of Wsep on the structural and electronic properties of the metal can be found.

We have studied the correlation between the interface Wsep and the corresponding strain in the metal slabs. When considering separately NST and ST, the Wsep is qualitatively well approximated by a linear function of the metal strain. In Fig. 3 the approximate linear dependence is shown for both the ST and NST and ZrO_2 and HfO_2 interfaces. ZrO_2 and HfO_2 have not only similar electronic configurations but also analogous crystal structures with close lattice parameters.[54] The ST interfaces not only present smaller values of Wsep than the NST ones but also their variations are smaller for a similar distortion of the 2D metal area. In general, from Fig. 3 it can be concluded that the Wsep is larger for interfaces with the metal under tensile strain. We have also analyzed the dependence of Wsep on the ratio between the bulk 2D unit cells of the metal and the ceramic. We obtain that the larger values of Wsep are found when the metal area is smaller than that of the ceramic, which again directly relates a high Wsep with a high metal tensile strain. Since the strain in the metal is tensile, a bond stretching in the metal layer induces an interface bond strengthening and thus increases the interface cohesion.

TABLE VII. Bonding overlap population (BOP) for the bulk structures of bcc and fcc metals of Tables III–V ordered by atomic numbers. The total charge for all the metals has been normalized to 1. See Ref. 17 for pseudopotential generation details.

fcc	BOP	bcc	BOP
Ni	0.107	Na	0.350
Cu	0.093	Nb	0.198
Rh	0.120	Mo	0.189
Pd	0.078	Ta	0.201
Ag	0.082	W	0.199
Pt	0.084		

Hybridization character and structure

Another correlation may be established between the Wsep and the electronic properties of the metal. In a solid the total charge of an atom can be decomposed into the Mulliken population and the bonding overlap populations.[73] While the former provides information on the electronic charge balance at each atomic site, the second may be viewed as the amount of charge shared in the bonds. Although both quantities are dependent on the choice of the basis set, they correctly give trends on the amount of charge transfer or the atomic hybridization as long as calculations are performed within a consistent scheme and are sufficiently accurate. Our calculations fulfill both criteria, allowing us to analyze the relation between the calculated Wsep and the metal bond overlap population (BOP).

Table VII provides the bulk metal BOP for the metals forming the calculated interfaces. Due to the localized nature of the d band, metals with a sp VB have larger BOP than

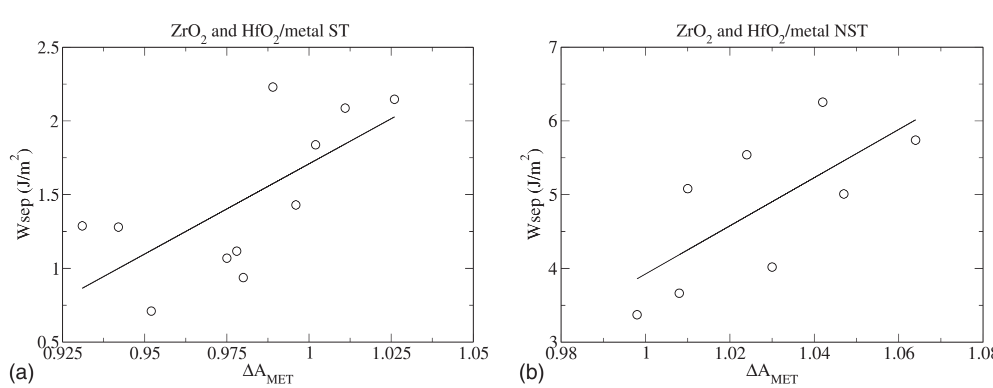

FIG. 3. Relation between the values of Wsep and ΔA_{MET} for the ST and NST interfaces formed by ZrO_2 and HfO_2 with different metals. The continuous lines correspond to a linear fit of the data. Notice the scale of the vertical axis on the right is twice smaller.

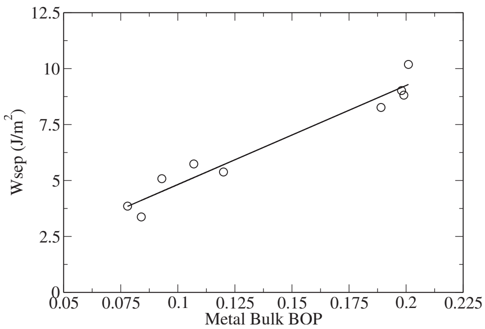

FIG. 4. Wsep versus the bulk metal BOP for the NST $ZrO_2(001)_O$ interfaces with different (001) metal structures, empty and full circles correspond to fcc and bcc structures, respectively.

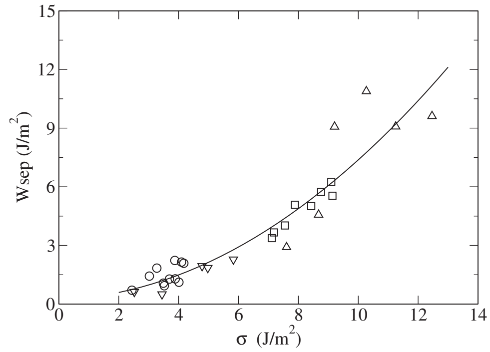

FIG. 5. Wsep vs $\langle\sigma\rangle = \langle\sigma_{MET}\rangle + \langle\sigma_{M_xO_y}\rangle$ for all calculated interfaces. The continuous line represents a quadratic fit to the data, circles (triangles down) corresponds to ST interfaces with misfit of less (more) than 10%, and squares (triangles up) to NST interfaces with misfit of less (more) than 10%.

those corresponding to metals with a VB formed mainly by *d* electrons. Even more, for larger number of *d* electrons the BOPs are smaller; then higher hybridization is shown for bcc than for fcc metals. On the other hand, the screening effects tend to increase the BOP with *Z* for a fixed number of *d* electrons, with the exceptions of Ni and Cu. This must be due to the fact that they are generated with the electronic configurations $4s^1 3d^9$ and $4s^1 3d^{10}$, respectively (see Ref. 17 for details in the pseudopotential generation). Figure 4 illustrates the dependence of the Wsep on the metal BOP for polar $ZrO_2(001)_O$/metal(001) interfaces. As previously stated, there is a large difference, around a factor of 2, between the Wsep for bcc and fcc metals. What Fig. 4 shows is that this large Wsep correlates with the larger values of the BOP for bcc metals, that is, with the available amount of charge shared in the metal bonds. In a first approximation the correlation can be considered as linear. Moreover, an analysis of the ionic character of the interface metal-O bonds indicates that most of the charge transfer originates from the interstitial metal bond charge.

Also, a relation between large metal BOP values and large Wsep is found for different ceramics and crystal orientations, as is the case of $Al_2O_3(0001)_O$. In general, this relation is valid regarding metals with a valence *d* band. However, for Na, showing the largest BOP among all metals, the Wsep at different MgO interfaces is lower than the corresponding value for Ag, with a significantly smaller BOP. On the other hand, the much slighter variations in the BOP when increasing *Z* for a fixed number of VB *d* electrons can also be correlated with the enhancement of Wsep.

VII. WORK OF SEPARATION VS SURFACE AND INTERFACE ENERGIES

As explained in the theoretical methodology, the ideal work of separation can be expressed in terms of the surface and interface free energies [see Eq. (1)].

Thus, the work of separation not only depends on the interface bonds but also on the properties of the surfaces involved. In fact, there is a correlation between Wsep and σ. We find that interfaces built from surfaces with large σ have larger Wsep than those containing surfaces with small σ. Figure 5 shows the Wsep as a function of the sum of the ceramic and metal surface energies, $\sigma = \sigma_{MET} + \sigma_{M_xO_y}$, for all the calculated interfaces. For polar surfaces, $\sigma_{M_xO_y}$ is taken as the mean value $\langle\sigma_{M_xO_y}\rangle$ within the range of allowed μ_O (see Sec. II). Accurate surface energies can only be obtained from calculations with ST ceramic slabs. However, in order to have identical terminations at both sides of the slab, NST slabs terminated in polar surfaces must be used. In this case $\sigma_{M_xO_y}$ is given as a function of the oxygen chemical potential μ_O. Nevertheless, due to the similar values of $\Delta G^f_{M_xO_y}$ for the oxides investigated in the present work, the general trend shown in Fig. 5 is almost unchanged regardless of the use of $\langle\sigma\rangle$ instead of σ. $\Delta G^f_{M_xO_y}$ takes the values −5.37, −5.76, and −5.79 eV for *c*-ZrO_2, *c*-HfO_2, and α-Al_2O_3, respectively.

Despite the great variety of interfaces investigated, the relation between Wsep and σ is parabolic. Note that in Fig. 5 we are including not only different metals, crystal structures, and interface coordinations but also different ceramics and consequently different bonding mechanisms, for example, charge transfer in O-metal bonds or hybridization in cation-metal interactions. A similar trend has been found from a systematic study of Al interfaces with Al_2O_3, nitrides, and carbides.[16]

Furthermore, from Fig. 5 it is evident that interfaces containing oxide polar surfaces with large σ and whose rupture requires the breaking of strong anion-cation ionic bonds present larger Wsep than those containing nonpolar surfaces. In fact, the formation of interface bonds, and consequently the modification of the surface charge, seems to be a reliable mechanism to decrease the σ and stabilizes polar surfaces, as indicated in their large reactivity.

If we restrict to HfO_2 and ZrO_2 (for which we have calculated the largest number of interfaces) and to result from NST slabs (an accurate comparison with ST slabs would require the precise knowledge of μ_O) the relation is linear, as shown in Fig. 6. Thus, Figs. 5 and 6 suggest that the summed surface energies of the oxide and the metal are the dominant terms in Eq. (1).

However, the interfacial energy γ contribution to Wsep, although relatively small, is not negligible as was previously proposed.[16] Figure 7 represents the dependence of Wsep on $\frac{\gamma}{\sigma}$, indicating that there are substantial differences between

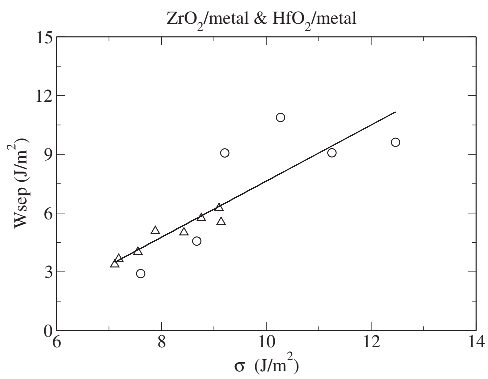

FIG. 6. Same as Fig. 5 for the polar interfaces formed only by HfO_2 or ZrO_2 ceramics. Triangles (circles) correspond to less (more) than 10% misfit between cell constituents.

ST and NST geometries. For ST interfaces γ is comparable to the surface energies, $\frac{\gamma}{\sigma}$ ranges from 0.4 to almost 0.9, and then the Wsep is not given by the surface energies alone. Nevertheless, for NST interfaces its contribution is not very important, since γ is small in comparison to the surface energies and even may take negative values indicating that interface bonds are as strong as those of the bulk metal and ceramic constituents, thus Wsep $\approx \sigma$. In particular, NST interfaces formed with bcc metals have the largest Wsep, around 10 J/m^2, almost independent of the constituents and of the $\frac{\gamma}{\sigma}$ value.

VIII. INTERFACE STABILITY

Besides Wsep, γ gives the excess free energy of an interface compared to the corresponding bulk materials, quantifying the strength of the interfacial bonds with respect to the bulk bonds. In addition, it allows one to know which interfaces are more stable in a thermodynamic sense. γ is calculated by Eq. (2) as a function of the oxygen chemical potential and therefore of the oxygen pressure.

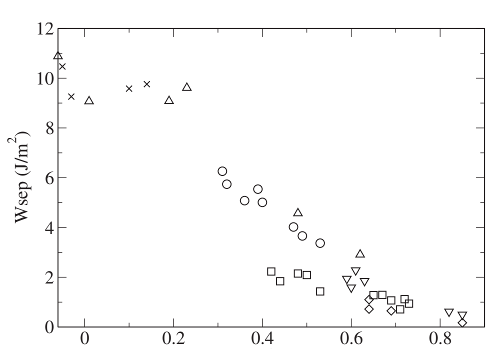

FIG. 7. Wsep vs $\langle\gamma/\sigma\rangle$ for all calculated interfaces. Crosses correspond to NST interfaces formed by O-terminated Al_2O_3 and bcc metals with lattice mismatch close to 10%. Inverted triangles correspond to ST ZrO_2/metal interfaces with more than 10% mismatch. Triangles correspond to NST $ZrO_2(001)$/metal interfaces with more than 10% mismatch. NST $ZrO_2(001)$ and $HfO_2(001)$ interfaces with fcc metals and less than 10% mismatch are represented by circles. Squares correspond to ST ZrO_2/metals with less than 10% mismatch. And rhombus indicate ST interfaces constituted by MgO with Ag or Na and mismatch close to 10%.

TABLE VIII. γ for interfaces formed by ST ceramic slabs and the corresponding Wsep, both values are given in J/m^2.

ST ceramic	γ	Wsep
$ZrO_2(111)_O/Ni(111)$ [a]	2.89	1.12
$HfO_2(111)_O/Ni(111)$	2.60	1.29
$ZrO_2(110)/Ni(100)$	2.59	0.94
$HfO_2(110)/Ni(100)$	2.46	1.07
$HfO_2(110)/Ni(110)$	2.09	2.09
$ZrO_2(111)_O/Ni(111)$ [b]	1.99	1.28
$ZrO_2(110)/Ni(110)$	1.95	2.15
$ZrO_2(110)/Cu(100)$	1.73	0.71
$ZrO_2(111)_O/Ta(100)$	1.64	2.23
$ZrO_2(110)/Cu(110)$	1.59	1.43
$ZrO_2(111)_O/Nb(100)$	1.43	1.84
MgO(110)/Ag(110)	1.99	1.10
MgO(110)/Na(110)	1.42	0.65
MgO(100)/Ag(100)	1.25	0.72
MgO(100)/Na(100)	0.96	0.17

[a] Aligned with in-plane directions $ZrO_2[1-10]/Ni[1-10]$ (Ref. 61).
[b] Aligned with in-plane directions $ZrO_2[1-34]/Ni[0-44]$ (Ref. 62).

Table VIII yields the calculated interface energy for the ST interfaces. All the values are positive indicating that the formation of the interface costs energy. The smallest values of γ—those for the most stable interfaces—correspond to MgO even though they also present the smaller Wsep. Similarly to the results obtained for the Wsep, the range of γ are close for the interfaces containing ZrO_2 and MgO, in fact, for the same metal and crystal orientations the interface ZrO_2 and MgO free energies differ by less than 10%. The most stable interface formed by the ZrO_2 and HfO_2 oxides corresponds to c-$ZrO_2(111)_O/Nb(100)$, which Wsep is also among the largest obtained for ST interfaces. However, the γ variations shown in Table VIII are not very large, indicating that the stabilities of the ST interfaces are analogous.

The calculated γ for the NST interfaces are represented in Tables IX and X, only for the two extreme values of $\Delta\mu_O$, 0, and $\frac{1}{y}\Delta G^f_{M_xO_y}$, which correspond to high and low oxygen pressures, respectively. γ varies linearly between these two extremes. For $\Delta\mu_O=0$ ($\frac{1}{y}\Delta G^f_{M_xO_y}$), i.e., high (low) oxygen pressures, the interfaces formed by the anion (cation) termination of the oxide are the most stable. Even more, many interfaces formed by the O-terminated oxides show at high O pressures negative values of γ, which evidences stronger bonds at the interface than those of the bulk structures. Moreover, the Al_2O_3/metal interfaces, containing the O-terminated Al_2O_3 surfaces, present very small γ values at rich O pressures, indicating a rather high stability of these interfaces.

IX. INTERFACE PROPERTIES BEYOND THE ELASTIC REGIME

The ideal Wsep, defined in Eq. (1), is the reversible work needed to separate the interface into two free surfaces if the

TABLE IX. Interface energies at $\Delta\mu_O=0$ and $\Delta\mu_O=\frac{\Delta G^f_{M_xO_y}}{y}$ for NST interfaces formed between fcc metals and ZrO_2 or HfO_2 oxides with less than 10% mismatch and bcc metals with $Al_2O_3(0001)$. It also includes the value of the Wsep for each interface and all values are given in J/m^2. The ΔG^f values for c-ZrO_2, c-HfO_2, and α-Al_2O_3 is −5.37, −5.76, and −5.79 eV, respectively.

NST ceramic	γ_0	$\gamma_{\frac{\Delta G^f_{M_xO_y}}{y}}$	Wsep
$Al_2O_3(0001)_O$/			
Ta(111)	−3.91	2.91	10.47
W(111)	−1.97	5.06	9.76
Mo(111)	−2.46	4.59	9.58
Nb(111)	−3.65	3.08	9.26
$ZrO_2(100)_O$/			
Ni(001)	−0.45	5.97	5.74
Cu(001)	−0.37	5.97	5.08
Rh(111)	0.31	6.76	4.02
Pt(111)	0.67	6.81	3.37
$ZrO_2(100)_{Zr}$/			
Ni(001)	6.65	0.13	5.01
Cu(001)	6.70	0.35	3.66
HfO_2/Ni(001)			
(100)O	−0.43	6.12	6.26
(100)Zr	6.63	0.26	5.54

plastic and diffusional degrees of freedoms are suppressed. Due to the neglect of these terms, Wsep always represents a lower bound for the fracture energy measured in any cleavage experiment.[17,65]

However some insight into the ability to mechanical reinforcement of a particular system can be gained by comparing the adhesion properties at the interface, characterized by Wsep, to those of the constituent materials.

Applying Eq. (1) for homogeneous materials, the work of separation needed to form two surfaces from the bulk structure is given by $\text{Wsep}_i=2\sigma_i$, where σ_i $(i=\text{MET},M_xO_y)$

TABLE X. Same as Table IX for the interfaces formed by fcc and bcc (001) metals with $ZrO_2(001)$ with more than 10% mismatch.

NST ceramic	γ_0	$\gamma_{\frac{\Delta G^f_{M_xO_y}}{y}}$	Wsep
$ZrO_2(100)_O$/			
Ta(100)	−3.97	2.74	10.88
W(100)	−0.68	6.41	9.61
Mo(100)	−1.23	5.51	9.08
Nb(100)	−3.24	3.43	9.07
Rh(100)	1.10	7.26	4.57
Pd(100)	1.65	7.78	2.91

TABLE XI. Wsep and surface energies of the ceramic and metal for NST interfaces with <10% mismatch. The underlined quantity indicates the region (ceramic, metal, or interface) where crack failure is expected to occur. All quantities are given in J/m^2.

NST ceramic	$2\sigma_{CER}$	$2\sigma_{MET}$	Wsep
$Al_2O_3(0001)_O$/			
Ta(111)	13.97	<u>5.97</u>	10.47
W(111)	14.43	<u>8.18</u>	9.76
Mo(111)	14.45	<u>6.84</u>	9.58
Nb(111)	13.78	<u>4.16</u>	9.26
$ZrO_2(100)_O$/			
Ni(001)	12.04	<u>5.48</u>	5.74
Cu(001)	12.48	<u>3.30</u>	5.08
Rh(111)	10.24	4.86	<u>4.02</u>
Pt(111)	10.80	3.42	<u>3.37</u>
$ZrO_2(100)_{Zr}$/			
Ni(001)	11.42	5.44	<u>5.01</u>
Cu(001)	11.16	<u>3.22</u>	3.66
HfO_2/Ni(001)			
(100)O	12.80	<u>5.40</u>	6.26
(100)Zr	12.91	<u>5.37</u>	5.54

stands for the surface energy of the material considered, either the metal or the ceramic. Therefore, from the knowledge of σ_{MET}, $\sigma_{M_xO_y}$, and the interface Wsep, it is possible to predict the place of failure of a heterogeneous interface in a cleavage experiment since it fails on the region of weakest bonds.

Tables XI and XII compile the adhesion values for different interfaces and the corresponding metal and oxide surface energies. For the NST ZrO_2 and HfO_2 surfaces (second block), all the Wsep values are higher than the metal surface energies except for $ZrO_2(100)_{Zr}$/Ni(001), $ZrO_2(100)_O$/Rh(111) and $ZrO_2(100)_O$/Pt(111). On the other hand, all the interfaces formed by the Al_2O_3 show Wsep values well above those of the metal surface energies. The average surface energy of the oxide is always larger. Therefore, it is expected that NST interfaces will commonly fail in the metal region. Contrarily, for interfaces built from ST surfaces, see Table XII, the Wsep is the smallest quantity but for MgO(110)/Na(110) and $ZrO_2(111)_O$/Ta(100). Therefore, they will fail at the interface, presenting brittle debonding.

We would like to point out that our calculations are valid under the elastic regime, beyond which is expected that the start of the metal plastic deformation contributes further to the reinforcement of the system.[74] In fact, many fracture experiments on α-Al_2O_3 and metals such as Nb, Al, Ni, Cu, or Au have shown toughening mechanisms such as the crack blunting, which is based on the plastic deformation of the metal and can induce fracture energies above 200 J/m^2 with no need of a very good interface matching.[5] A summary of the experimental measurements is shown in Ref. 75. Particu-

TABLE XII. Same as Table XI but for ST interfaces. All quantities are given in J/m^2.

ST ceramic	$2\sigma_{CER}$	$2\sigma_{MET}$	Wsep
$ZrO_2(111)_O$/			
Ta(100)	2.02	5.72	2.23
Nb(100)	2.04	4.50	1.84
Ni(111)[a]	3.32	4.70	1.12
Ni(111)[b]	2.46	4.92	1.28
ZrO_2(110)/			
Ni(110)	2.84	5.36	2.15
Cu(110)	2.66	3.38	1.43
Ni(100)	1.72	5.34	0.94
Cu(100)	1.58	3.30	0.71
HfO_2/Ni			
(110)/(110)	2.90	5.44	2.09
$(111)_O/(111)$	2.74	5.04	1.29
(110)/(100)	1.62	5.36	1.07
MgO/Ag			
(110)/(110)	4.08	2.11	1.10
(100)/(100)	1.74	2.19	0.72
MgO/Na			
(110)/(110)	3.70	0.45	0.65
(100)/(100)	1.78	0.48	0.17

[a]Aligned with in-plane directions $ZrO_2[1-10]/Ni[1-10]$ (Ref. 61).
[b]Aligned with in-plane directions $ZrO_2[1-34]/Ni[0-44]$ (Ref. 62).

larly, a reported fracture energy of 112 ± 51 J/m^2 has been found for the $Al_2O_3(0001)/Nb(111)$ interface, indicating that a mechanism of plasticity may occur.[76]

The α-$Al_2O_3(0001)/Mo(111)$ interface has also been studied in cermets formed by a polycrystalline ceramic matrix including metal particles.[77] An increase in the fracture energy from 20 to 60 J/m^2 is obtained when the concentration of the metal increases from near 0% to 20%, with a bridging mechanism induced by ductile particles. Our results again compare qualitatively well since we obtain plastic reinforcement in this system. Therefore, although plasticity effects are not taken specifically into account in our calculations, we expect from Tables XI and XII a plastic reinforcement for every bcc metal when forming interfaces with α-$Al_2O_3(0001)$, in agreement with the available experimental measurements.

Furthermore, we consider another criterion of interface failure based on the stress intensity that settles the start of plastic deformation in the metal. The local stress intensity (Kie) needed for the emission of the first dislocation, and therefore the beginning of the plastic regime, has been obtained by a three-dimensional (3D) molecular-dynamics simulation for various fcc metals.[78] The available values for the fcc metals, involved in the interfaces described in Tables XI and XII, are given in Table XIII together with the phenomenological stress intensity assigned to the interface (K_{IC}) as derived from our calculated Wsep,[74]

$$K_{IC} = \sqrt{\frac{\mathrm{Wsep} E_{\mathrm{Young}}}{(1-\nu^2)}},$$

where ν is the Poisson modulus and E_{Young} is the Young modulus of the constituent metals. The Poisson modulus for polycrystalline metals is fairly constant and close to 0.33, which is the value we employ for all the metals. The value of K_{IC} calculated from the metal parameters gives the lowest limit of the interface stress intensity since K_{IC} obtained from the oxide parameters is always larger.

If $K_{IC} > \mathrm{Kie}$ dislocations are formed at the metal side and the mechanical properties of the complete interface are improved by a toughening mechanism. From the Table XIII we can see that for NST interfaces K_{IC} is generally larger than Kie, being both stress intensity values rather similar, while for the ST cases K_{IC} is around two times smaller than Kie. These results compare well with those previously obtained in

TABLE XIII. Stress intensity (K_{IC}) of the interfaces with $<10\%$ of mismatch and formed by fcc metals to compare with the available local stress intensity (Kie) values of the metal (Ref. 78), both values given in MPa $\sqrt{m}$.

NST ceramic	K_{IC}	Kie
$MxO_2/Ni(001)$		
$HfO_2(100)_O$	1.18	1.10
$ZrO_2(100)_O$	1.11	1.10
$HfO_2(100)_{Hf}$	1.13	1.10
$ZrO_2(100)_{Zr}$	1.06	1.10
$MxO_2/Cu(001)$		
$ZrO_2(100)_O$	0.86	0.71
$ZrO_2(100)_{Zr}$	0.73	0.71
$ZrO_2(100)_O/Pt(111)$	0.80	0.63
ST ceramic		
MxO_2/Ni		
$ZrO_2(110)/(110)$	0.69	1.10
$HfO_2(110)/(110)$	0.68	1.10
$HfO_2(111)_O/(111)$	0.54	1.10
$ZrO_2(111)_O/(111)$ [a]	0.54	1.10
$ZrO_2(111)_O/(111)$ [b]	0.50	1.10
$HfO_2(110)/(100)$	0.49	1.10
$ZrO_2(110)/(100)$	0.46	1.10
MxO_2/Cu		
$ZrO_2(110)/(110)$	0.46	0.71
$ZrO_2(110)/(100)$	0.32	0.71

[a]Aligned with in-plane directions $ZrO_2[1-10]/Ni[1-10]$ (Ref. 61).
[b]Aligned with in-plane directions $ZrO_2[1-34]/Ni[0-44]$ (Ref. 62).

Tables XI and XII and tell us that an enhancement of the adhesion by the bridging mechanism may occur in almost all NST interfaces.

X. CONCLUSIONS

A systematic investigation of the adhesion properties of a broad range of oxide/metal interfaces has been performed by *ab initio* DFT methods. General trends of the behavior of Wsep, which characterizes the mechanical properties of the oxide/metal system in the elastic regime as a function of the charge, structure, and strain conditions of the constituent materials are established.

Differences as large as one order of magnitude in the Wsep have been obtained depending on the surface of the oxide. The higher Wsep are found for nonstoichiometric geometries, which mainly correspond to O-terminated oxide polar surfaces. While stoichiometric interfaces, related to nonpolar oxide terminations, present Wsep values substantially smaller than those corresponding to the nonstoichiometric surfaces. Moreover, the crystal structure of the transition metal also influences the Wsep resulting in general in higher values for bcc than for fcc transition metals. Further, the strain conditions affect the interface adhesion and larger values of Wsep are found for strained configurations. The calculated Wsep's follow a parabolic dependence on the summed surface energies of the metal and the oxide regardless of the oxide and metal components, crystal lattice, orientations, or atomic terminations. The interfacial energy contribution to Wsep, although non-negligible, is smaller compared to the surface energy contribution, especially for nonstoichiometric geometries which show the largest Wsep.

In addition, an attempt to analyze the nonelastic fracture mechanisms is also accomplished. The comparison of the interface crack resistance and those associated to the metal and oxide bulk allows us to estimate the region of failure of the system and to discuss whether a reinforcement of the mechanical properties by plastic deformation of the metal takes place. Our analysis indicates that interfaces formed by nonstoichiometric oxides are frequently reinforced by plastic mechanisms, while for stoichiometric geometries the oxide/metal interface fails by decohesion and no plasticity reinforcement is obtained.

ACKNOWLEDGMENTS

We are very grateful to J.F. Bartolomé, S. Gallego, C. Pecharromán, and J.S. Moya for many fruitful discussions. This work was supported by the Spanish Ministry of Education and Science under Project No. MAT2006-05122.

*juan.beltran@materianova.be

[1] S. Roberts and R. J. Gorte, J. Phys. Chem. **95**, 5600 (1991).
[2] H. Kim, P. C. McIntyre, C. O. Chui, K. C. Saraswat, and S. Stemmer, J. Appl. Phys. **96**, 3467 (2004).
[3] http://www.kmm-noe.org/DesktopDefault.aspx?tabindex=75&=219
[4] B. Lawn, *Fracture of Brittle Solids* (Cambridge University Press, Cambridge, 1993).
[5] A. G. Evans, D. R. Mumm, J. W. Hutchinson, G. H. Meier, and F. S. Pettit, Prog. Mater. Sci. **46**, 505 (2001).
[6] J. F. Bartolomé, J. I. Beltrán, C. F. Gutiérrez-González, C. Pecharromán, M. C. Muñoz, and J. S. Moya, Acta Mater. **56**, 3358 (2008).
[7] C. Pecharromán, J. I. Beltrán, F. Esteban-Betegón S. López-Esteban, J. F. Bartolomé, M. C. Muñoz, and J. S. Moya, Z. Metallkd. **96**, 507 (2005).
[8] S. B. Sinnott and E. C. Dickey, Mater. Sci. Eng., R. **43**, 1 (2003).
[9] I. G. Batyrev, A. Alavi, and M. W. Finnis, Phys. Rev. B **62**, 4698 (2000).
[10] M. Lane, Annu. Rev. Mater. Res. **33**, 29 (2003).
[11] A. G. Evans and B. J. Dalgleish, Mater. Sci. Eng., A **162**, 1 (1993).
[12] R. Grau-Crespo, N. Cruz Hernández, J. F. Sanz, N. H. de Leeuw, J. Phys. Chem. C **111**, 10448 (2007).
[13] M. Alfredsson and C. R. A. Catlow, Phys. Chem. Chem. Phys. **4**, 6100 (2002).
[14] W. Zhang, J. R. Smith, and A. G. Evans, Acta Mater. **50**, 3803 (2002).
[15] A. Bogicevic and D. R. Jennison, Phys. Rev. Lett. **82**, 4050 (1999).
[16] D. J. Siegel, L. G. Hector, Jr., and J. B. Adams, Phys. Rev. B **67**, 092105 (2003).
[17] M. C. Muñoz, S. Gallego, J. I. Beltrán, and J. Cerdá, Surf. Sci. Rep. **61**, 303 (2006).
[18] J. I. Beltrán, S. Gallego, J. Cerdá, J. S. Moya, and M. C. Muñoz, Phys. Rev. B **68**, 075401 (2003).
[19] J. I. Beltrán, S. Gallego, J. Cerdá, J. S. Moya, and M. C. Muñoz, J. Phys. Chem. B **108**, 15439 (2004).
[20] J. M. Soler, E. Artacho, J. D. Gale, A. Garcia, J. Junquera, P. Ordejón, and D. Sánchez-Portal, J. Phys.: Condens. Matter **14**, 2745 (2002).
[21] P. Hohenberg and W. Kohn, Phys. Rev. **136**, B864 (1964).
[22] W. Koch and M. C. Holthausen, *A Chemist's Guide to Density Functional Theory* (WCH-Wiley, Weinheim, 2001).
[23] J. P. Perdew, K. Burke, and M. Ernzerhof, Phys. Rev. Lett. **77**, 3865 (1996).
[24] H. J. Monkhorst and J. D. Pack, Phys. Rev. B **13**, 5188 (1976).
[25] V. N. Staroverov, G. E. Scuseria, J. Tao, and J. P. Perdew, Phys. Rev. B **69**, 075102 (2004).
[26] J. H. Cho and M. Scheffler, Phys. Rev. B **53**, 10685 (1996).
[27] http://www.webelements.com/.
[28] S. Curtarolo, D. Morgan, and G. Ceder, Calphad **29**, 163 (2005).
[29] J. C. Bailor, H. J. Emeleus, R. S. Nyholm, and A. F. Trotman-Dickenson, *Comprehensive Inorganic Chemistry* (Pergamon Press, Oxford, 1973).
[30] E. Wachowicz and A. Kiejna, J. Phys.: Condens. Matter **13**, 10767 (2001).
[31] F. Willaime, J. Nucl. Mater. **323**, 205 (2003).
[32] A. S. Foster, F. Lopez Gejo, A. L. Shluger, and R. M. Nieminen,

Phys. Rev. B **65**, 174117 (2002).
[33] J. Malcolm W. Chase, Jr., *NIST-JANAF Themochemical Tables, Fourth Edition, J. Phys. Chem. Ref. Data*, Monograph 9 (1998).
[34] D. J. Siegel, Ph.D. thesis, University of Illinois, 2001.
[35] W. Y. Ching and Y.-N. Xu, J. Am. Ceram. Soc. **77**, 404 (1994).
[36] *CRC Handbook of Chemistry and Physics*, 67th ed., edited by R. C. Weast (CRC, Boca Raton, FL, 1983).
[37] P. Richet, J. Xu, and H. K. Mao, Phys. Chem. Miner. **16**, 207 (1988).
[38] H. d'Amour, D. Schiferl, W. Denner, H. Schulz, and W. B. Holzapfel, J. Appl. Phys. **49**, 4411 (1978).
[39] G. Geneste, J. Morillo, and F. Finocchi, Appl. Surf. Sci. **188**, 122 (2002).
[40] A. R. Oganov and P. I. Dorogokupets, Phys. Rev. B **67**, 224110 (2003).
[41] J. Kang, E.-C. Lee, and K. J. Chang, Phys. Rev. B **68**, 054106 (2003).
[42] I. M. Iskandarova, A. A. Knizhnik, E. A. Rykova, A. A. Bagatur'yants, B. V. Potapkin, and A. A. Korkin, Microelectron. Eng. **69**, 587 (2003).
[43] J. E. Lowther, J. K. Dewhurst, J. M. Leger, and J. Haines, Phys. Rev. B **60**, 14485 (1999).
[44] N. I. Mednedeva, V. P. Zhukov, M. Y. Khodos, and V. A. Gubanov, Phys. Status Solidi B **160**, 517 (1990).
[45] G. Jomard, T. Petit, A. Pasturel, L. Magaud, G. Kresse, and J. Hafner, Phys. Rev. B **59**, 4044 (1999).
[46] A. S. Foster, V. B. Sulimov, F. Lopez Gejo, A. L. Shluger, and R. M. Nieminen, Phys. Rev. B **64**, 224108 (2001).
[47] L. K. Dash, N. Vast, P. Baranek, M.-C. Cheynet, and L. Reining, Phys. Rev. B **70**, 245116 (2004).
[48] S. Fabris, A. T. Paxton, and M. W. Finnis, Phys. Rev. B **61**, 6617 (2000).
[49] E. V. Stefanovich, A. L. Shluger, and C. R. A. Catlow, Phys. Rev. B **49**, 11560 (1994).
[50] P. Aldebert and J.-P. Traverse, J. Am. Ceram. Soc. **68**, 34 (1985).
[51] C. J. Howard, R. J. Hill, and B. E. Reichert, Acta Crystallogr. B **B44**, 116 (1988).
[52] R. J. Ackermann, E. G. Rauh, and C. A. Alexander, High. Temp. Sci. **7**, 304 (1975).
[53] R. P. Ingel and D. Lewis III, J. Am. Ceram. Soc. **71**, 265 (1988).
[54] V. Fiorentini and G. Gulleri, Phys. Rev. Lett. **89**, 266101 (2002).
[55] N. Sanchez, S. Gallego, and M. C. Muñoz (unpublished).
[56] I. G. Batyrev, A. Alavi, and M. W. Finnis, Phys. Rev. B **62**, 4698 (2000).
[57] K. Reuter and M. Scheffler, Phys. Rev. B **65**, 035406 (2001).
[58] J. I. Beltrán, Ph.D. thesis, University Auton Madrid, 2007.
[59] J. I. Beltrán, M. C. Muñoz, and J. Hafner, New J. Phys. **10**, 063031 (2008).
[60] J. I. Beltrán, S. Gallego, J. Cerdá, and M. C. Muñoz, J. Eur. Ceram. Soc. **23**, 2737 (2003).
[61] T. Sasaki, K. Matsunaga, H. Ohta, H. Hosono, T. Yamamoto, and Y. Ikuhara, Mater. Trans. **45**, 2137 (2004).
[62] A. Christensen and E. A. Carter, J. Chem. Phys. **114**, 5816 (2001).
[63] A. Eichler and G. Kresse, Phys. Rev. B **69**, 045402 (2004).
[64] P. W. Tasker, J. Phys. C **12**, 4977 (1979).
[65] M. W. Finnis, J. Phys.: Condens. Matter **8**, 5811 (1996).
[66] C. Li, R. Wu, A. J. Freeman, and C. L. Fu, Phys. Rev. B **48**, 8317 (1993).
[67] U. Schönberger, O. K. Andersen, and M. Methfessel, Acta Metall. Mater. **40**, S1 (1992).
[68] E. Heifets, R. Orlando, R. Dovesi, C. Pisani, and E. A. Kotomin, *Second International Conference on Computer Simulation Radiation Effects in Solids* (Santa Barbara, 1994).
[69] T. Hong, J. R. Smith, and D. J. Srolovitz, J. Adhes. Sci. Technol. **8**, 837 (1994).
[70] A. Trampert, F. Ernst, C. P. Flynn, H. F. Fischmeister, and M. Rühle, Acta Metall. Mater. **40**, S227 (1992).
[71] J. A. Snyder, J. E. Jaffe, M. Gutowski, Z. Lin, and A. C. Hess, J. Chem. Phys. **112**, 3014 (2000).
[72] N. Eustathopoulos and B. Drevet, Mater. Sci. Eng., A **249**, 176 (1998).
[73] R. Hoffmann, *Solids and Surfaces: A Chemist's View of Bonding in Extended Structures* (VCH-Wiley, New York, 1988).
[74] J. E. Raynolds, J. R. Smith, G.-L. Zhao, and D. J. Srolovitz, Phys. Rev. B **53**, 13883 (1996).
[75] A. G. Evans, J. W. Hutchinson, and Y. Wei, Acta Mater. **47**, 4093 (1999).
[76] G. Soyez, G. Elssner, M. Rühle, and R. Raj, Acta Mater. **46**, 3571 (1998).
[77] O. Sbaizero, G. Pezzotti, and T. Nishida, Acta Mater. **46**, 681 (1998).
[78] J. Knap and K. Sieradzki, Phys. Rev. Lett. **82**, 1700 (1999).